Analysis and Implementation for Physical-Layer Network Coding with Carrier Frequency Offset

Meng Wu*, Frank Ludwig†, Matthias Woltering*, Dirk Wübben*, Armin Dekorsy*, and Steffen Paul†
*Department of Communications Engineering, University of Bremen, 28359 Bremen, Germany
Email: {wu, woltering, wuebben, dekorsy}@ant.uni-bremen.de
†Department of Communication Electronics, University of Bremen, 28359 Bremen, Germany
Email: {ludwig, steffen.paul}@me.uni-bremen.de

***Abstract*—In this paper we consider physical-layer network coding (PLNC) in OFDM-based two-way relaying systems. Practically, a key impairment for the application of PLNC is the carrier frequency offset (CFO) mismatch between the sources and the relay, which can not be compensated completely in the multiple-access (MA) phase. As this CFO mismatch results in inter-carrier interference (ICI) for OFDM transmissions, practical CFO compensation and ICI cancelation strategies are investigated to mitigate the impairment for a-posterior probability (APP) based PLNC decoders at the relay. Furthermore, we perform hardware implementation of the two-way relaying network employing an long term evolution (LTE) near parametrization adapted to PLNC. The APP-based decoding schemes with CFO compensation and ICI cancelation are applied on this real-time transmission platform to verify the analytical results.**

I. Introduction

In two-way relaying systems applying physical-layer network coding (PLNC) [1], two sources intend to exchange messages with each other helped by a relay. In the multiple-access (MA) phase, both sources transmit to the relay simultaneously. The relay estimates a network coded message from the receive signal and sends it back to the sources in the broadcast (BC) phase. Assuming perfect synchronization for the MA transmission, a-posterior probability (APP) based decoding schemes at the relay were developed to estimate the relay codeword in [2], [3]. In practical systems, there exists carrier frequency offset (CFO) between the signals at the transmitter and the receiver, which causes inter-carrier interference (ICI) for orthogonal frequency division multiplexing (OFDM) transmissions. For point-to-point transmissions, the CFO can be compensated completely considering perfect CFO estimation. However, the MA transmission for PLNC results in two CFOs between the signals from both sources and the relay. These two CFOs, if not matched, can not be compensated totally even if both are perfectly estimated. Such a CFO mismatch for PLNC jeopardizes the performance of the APP-based decoding schemes severely and thus has to be coped with properly. In [4], [5] the impairment caused by CFO mismatch was analytically studied for multi-user MIMO scenarios. A threshold-based ICI cancelation method was presented that subtracts the reconstructed ICI from the receive signal for re-detection in uncoded systems in [6]. A more sophisticated scheme employing the space-alternating generalized expectation-maximization (SAGE) algorithm [7] to combat the CFO mismatch is referred to [8]. Furthermore, the concept of PLNC in OFDM-based two-phase two-way relaying systems with CFO impacts has been brought to hardware implementation on the universal soft radio peripheral (USRP) [9] platform in [10], where a simple average CFO compensation strategy was proposed that effectively suppresses the total ICI.

In this work, practical CFO compensation as well as ICI cancelation strategies adapted to the APP-based decoders in [3] are investigated, which lead to robust performance against CFO mismatch for coded OFDM based PLNC. In order to verify the analytical results under a realistic system setup, we initiate a hardware implementation of the MA phase in two-way relaying communications using the Lyrtech hardware testbed [11] with a long term evolution (LTE) near parametrization adapted to PLNC. Both CFO compensation and ICI cancelation are performed that mitigate the impact of CFO mismatch effectively for real-time transmissions.

The remainder of this paper is organized as follows. In Section II, the system model is introduced with CFO mismatch. The APP-based PLNC decoding schemes are shortly reviewed in Section III and the CFO compensation and ICI cancelation strategies adapted to these APP-based schemes are demonstrated in Section IV. Performance evaluations of these strategies to cope with the CFO mismatch is included in Section V. In Section VI, hardware implementation of the MA phase for PLNC is discussed, where the presented strategies are verified using our real-time transmission platform. Finally, Section VII concludes the paper.

II. System Description

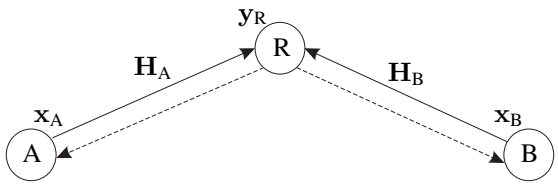

Fig. 1. A two-phase two-way relaying network consisting of a MA phase (solid lines) and a BC phase (dashed lines).

We consider a two-phase two-way relaying system shown in Fig. 1, where two sources A and B intend to exchange mes-

ISBN 978-3-8007-3584-6

sages with each other via a relay R. It is assumed that all nodes are equipped with a single antenna and OFDM transmissions are adopted. In the MA phase, A and B encode their binary information words $\mathbf{b}_\mathrm{A}$ and $\mathbf{b}_\mathrm{B}$ with the same linear channel code Γ of rate R_C, which results in the *source codewords* $\mathbf{c}_\mathrm{A} = \Gamma(\mathbf{b}_\mathrm{A})$ and $\mathbf{c}_\mathrm{B} = \Gamma(\mathbf{b}_\mathrm{B})$. Subsequently, both codewords are mapped to OFDM symbol vectors $\mathbf{x}_\mathrm{A} = \mathcal{M}(\mathbf{c}_\mathrm{A})$ and $\mathbf{x}_\mathrm{B} = \mathcal{M}(\mathbf{c}_\mathrm{B})$ of length N_C using a mapper $\mathcal{M}$, which are transmitted to R simultaneously. Denoting N_C the total number of subcarriers, the $N_\mathrm{C} \times 1$ receive signal vector $\mathbf{y}_\mathrm{R}$ for one whole OFDM symbol in frequency domain is given by

$$\mathbf{y}_\mathrm{R} = \mathbf{H}_\mathrm{A}\mathbf{x}_\mathrm{A} + \mathbf{H}_\mathrm{B}\mathbf{x}_\mathrm{B} + \mathbf{n}_\mathrm{R} \tag{1}$$

when the CFOs in both links are absent. The frequency selective channels are assumed to be Rayleigh block fading containing N_H equal power taps in time domain. Correspondingly, $\mathbf{H}_i$ in (1) denotes the $N_\mathrm{C} \times N_\mathrm{C}$ diagonal channel matrix in frequency domain, $i = \mathrm{A}, \mathrm{B}$, where each diagonal entry of $\mathbf{H}_i$ represents a subcarrier wise channel coefficient with variance $\sigma_h^2 = 1/N_\mathrm{H}$. Furthermore, $\mathbf{n}_\mathrm{R}$ denotes the $N_\mathrm{C} \times 1$ complex additive white Gaussian noise (AWGN) vector, each entry of which has zero mean and variance σ_n^2.

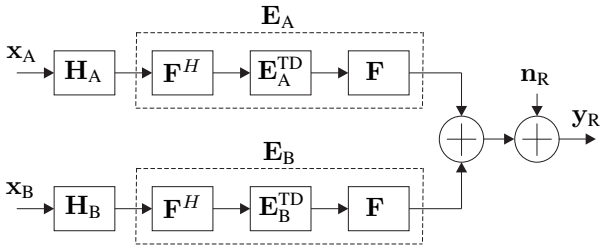

Fig. 2. System block diagram of the MA phase with respect to (2a) including the impact of CFO for one whole OFDM symbol vector.

With the presence of CFOs, the channels in the MA phase are distorted. Using the CFO model in [4], [5], the system equation (1) is rewritten as

$$\begin{aligned}\mathbf{y}_\mathrm{R} =& \mathbf{E}_\mathrm{A}\mathbf{H}_\mathrm{A}\mathbf{x}_\mathrm{A} + \mathbf{E}_\mathrm{B}\mathbf{H}_\mathrm{B}\mathbf{x}_\mathrm{B} + \mathbf{n}_\mathrm{R} && \text{(2a)}\\ =& \underbrace{\mathbf{\Lambda}_\mathrm{A}\mathbf{x}_\mathrm{A} + \mathbf{\Lambda}_\mathrm{B}\mathbf{x}_\mathrm{B}}_{\text{desired signal}} + \underbrace{\overline{\mathbf{\Lambda}}_\mathrm{A}\mathbf{x}_\mathrm{A} + \overline{\mathbf{\Lambda}}_\mathrm{B}\mathbf{x}_\mathrm{B}}_{\text{ICI}} + \mathbf{n}_\mathrm{R}\,. && \text{(2b)}\end{aligned}$$

The corresponding system block diagram is shown in Fig. 2. Therein, the CFO between each source and the relay is covered by $\mathbf{E}_i = \mathbf{F}\mathbf{E}_i^\mathrm{TD}\mathbf{F}^H$ with dimension $N_\mathrm{C} \times N_\mathrm{C}$. Here, $\mathbf{F}$ represents the $N_\mathrm{C} \times N_\mathrm{C}$ discrete Fourier transform (DFT) matrix, which is unitary and thus $\mathbf{F}\mathbf{F}^H$ is equal to the identity matrix $\mathbf{I}$. The $N_\mathrm{C} \times N_\mathrm{C}$ CFO distortion matrix $\mathbf{E}_i^\mathrm{TD}$ is diagonal and defined in time domain as

$$\mathbf{E}_i^\mathrm{TD} = \mathrm{diag}\left[1 \quad \mathrm{e}^{\frac{j2\pi\epsilon_i}{N_\mathrm{C}}} \quad \cdots \quad \mathrm{e}^{\frac{j2\pi\epsilon_i(N_\mathrm{C}-1)}{N_\mathrm{C}}}\right]. \tag{3}$$

Here, ϵ_i denotes the CFO normalized to subcarrier spacing, which is assumed to be perfectly known at the relay in this paper. Note that without CFO, i.e., $\epsilon_i = 0$, $\mathbf{E}_i$ is reduced to an identity matrix. Therefore, the orthogonality of the channel matrix $\mathbf{H}_i$ is preserved. However, this orthogonality is destroyed by the non-diagonal matrix $\mathbf{E}_i$ if $\epsilon_i \neq 0$, resulting in ICI described by the interference matrix $\overline{\mathbf{\Lambda}}_i$ as shown in (2b). The desired signal corresponds to the diagonal matrix $\mathbf{\Lambda}_i$ with the equivalent channel matrix $\mathbf{E}_i\mathbf{H}_i = \mathbf{\Lambda}_i + \overline{\mathbf{\Lambda}}_i$.

Upon reception at relay R, the *relay codeword* $\mathbf{c}_\mathrm{R}$ corresponding to the XORed packet is estimated from $\mathbf{y}_\mathrm{R}$, which is then broadcast to the sources in the broadcast (BC) phase. Due to the fact that A and B are aware of what they have transmitted in the MA phase, this self-interference can be completely removed by XOR operation with the estimated relay codeword $\hat{\mathbf{c}}_\mathrm{R}$ to retrieve the desired message.

III. APP-based Decoding Schemes

As decoding errors at the relay will propagate to the sources in the BC phase and thus degrade the overall system performance, we focus on the critical MA phase. To this end, APP-based decoding schemes for PLNC have been presented in [3] to estimate the relay codeword $\mathbf{c}_\mathrm{R}$ assuming no CFO impact, i.e., $\epsilon_i = 0$. These APP-based PLNC decoding schemes are shortly recaptured as follows.

A. Separated Channel Decoding (SCD)

For parallel SCD (P-SCD) both source codewords $\mathbf{c}_\mathrm{A}$ and $\mathbf{c}_\mathrm{B}$ are estimated explicitly in parallel, followed by network coding $\mathbf{c}_\mathrm{R} = \hat{\mathbf{c}}_\mathrm{A} \oplus \hat{\mathbf{c}}_\mathrm{B}$. Alternatively, successive SCD (S-SCD) subtracts the reconstructed signal component using the decoding result of the channel with larger fading gain, e.g., $\hat{\mathbf{c}}_\mathrm{A}$, from the receive signal and performs a common decoding with respect to this interference reduced signal to estimate $\hat{\mathbf{c}}_\mathrm{B}$.

B. Joint Channel Decoding and Physical-Layer Network Coding (JCNC)

For PLNC the relay is not interested in the individual source messages $\mathbf{c}_\mathrm{A}$ and $\mathbf{c}_\mathrm{B}$ but only forwards a network coded signal. Furthermore, since both sources employ the same linear channel code, the XORed message is also a valid codeword in the codebook. In these contexts, the relay is able to directly estimate $\mathbf{c}_\mathrm{R}$ from the receive signal $\mathbf{y}_\mathrm{R}$.

C. Generalized Joint Channel Decoding and Physical-Layer Network Coding (G-JCNC)

Since JCNC fails to fully exploit the coding gain provided by the two channel codes applied at the sources, G-JCNC originated from [2] directly feeds the APPs to a non-binary channel decoder. The updated APPs are used for PLNC to obtain the relay codeword $\mathbf{c}_\mathrm{R}$.

IV. CFO Compensation and ICI Cancelation

As the CFO mismatch between the sources and the relay leads to ICI, which destroys the orthogonality of OFDM transmissions, this impairment has to be considered adequately and mitigated for PLNC. Firstly, the CFOs can be compensated in time domain directly after signal reception at the relay. Afterwards, ICI stemming from the remaining CFOs can be reconstructed and canceled out in frequency domain. In this section, these two aspects are discussed for different decoding schemes presented in Section III to alleviate the impairment caused by CFO misalignment.

ISBN 978-3-8007-3584-6

A. CFO Compensation

Unlike complete CFO compensation in point-to-point communications, nulling both CFOs at relay R for the MA transmission in (2) is impossible if $\epsilon_A \neq \epsilon_B$. For instance, complete compensation of ϵ_A for the link from A to R results in $\epsilon'_A = 0$ and $\epsilon'_B = \epsilon_B - \epsilon_A \neq 0$, where ϵ'_i denotes the remaining CFO after compensation.

Alternatively, an average CFO compensation strategy by $-\frac{\epsilon_A+\epsilon_B}{2}$ introduced in [10] can be applied before applying the APP-based decoding schemes. Such a compensation strategy yields both remaining CFOs as

$$\epsilon'_A = \epsilon_A - \frac{\epsilon_A + \epsilon_B}{2} = \frac{\epsilon_A - \epsilon_B}{2} \tag{4a}$$

$$\epsilon'_B = \epsilon_B - \frac{\epsilon_A + \epsilon_B}{2} = \frac{\epsilon_B - \epsilon_A}{2} \,. \tag{4b}$$

In order to compare the two aforementioned CFO compensation strategies, a numerical example is presented with $N_C = 16$ subcarriers. Setting the original CFOs to $\epsilon_A = -0.05$ and $\epsilon_B = 0.15$, the corresponding graphical patterns of both equivalent channel gain matrices are shown in Fig. 3 without CFO compensation. Obviously, ϵ_B results in severer ICI in contrast to ϵ_A. Similar graphs are shown in Fig. 4 and Fig. 5 for the cases with complete compensation of ϵ_A and average compensation (4), respectively. When complete compensation of ϵ_A is adopted, which leads to $\epsilon'_A = 0$ and $\epsilon'_B = 0.2$, ICI totally disappears in Fig. 4(a) but increases significantly in Fig. 4(b). This indicates that complete compensation of one CFO amplifies its counterpart dramatically in this case. For average CFO compensation with $\epsilon'_A = -0.1$ and $\epsilon'_B = 0.1$, a compromise is achieved between the two CFOs that suppresses the larger CFO while not amplifying the smaller CFO too much, as shown in Fig. 5.

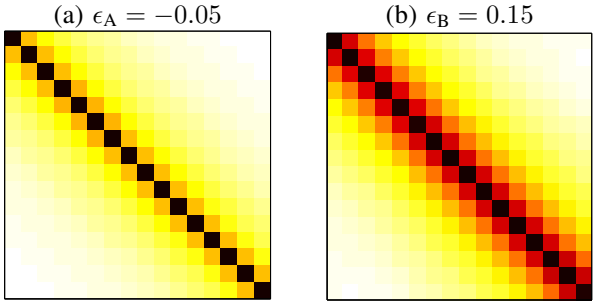

Fig. 3. Graphical patterns of both equivalent channel gain matrices in the MA phase before CFO compensation, $\epsilon_A = -0.05$ and $\epsilon_B = 0.15$.

Note that both ICI components $\overline{\mathbf{\Lambda}}_A$ and $\overline{\mathbf{\Lambda}}_B$ defined in (2b) contribute to impairment that degrades the performance of the initial detection for all PLNC decoding schemes. Therefore, the total ICI power P_{ICI} is plotted with respect to the relative CFO $|\epsilon_A - \epsilon_B|$ for both CFO compensation strategies in Fig. 6. As expected, average compensation leads to less amount of total ICI compared to complete compensation of one CFO especially for increasing relative CFO.

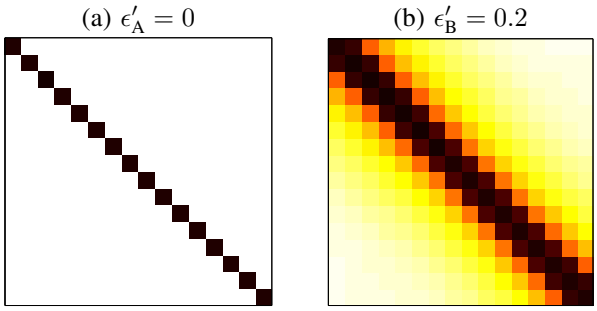

Fig. 4. Graphical patterns of both equivalent channel gain matrices in the MA phase after complete CFO compensation of ϵ_A, $\epsilon'_A = 0$ and $\epsilon'_B = 0.2$.

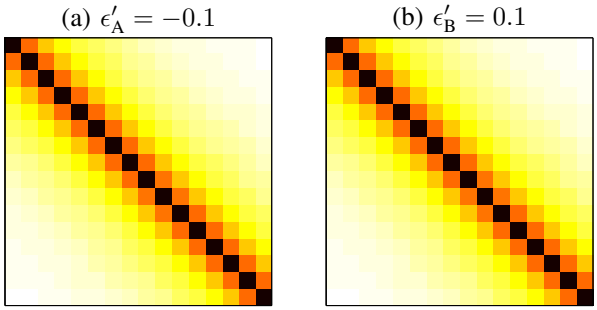

Fig. 5. Graphical patterns of both equivalent channel gain matrices in the MA phase after average CFO compensation, $\epsilon'_A = -0.1$ and $\epsilon'_B = 0.1$.

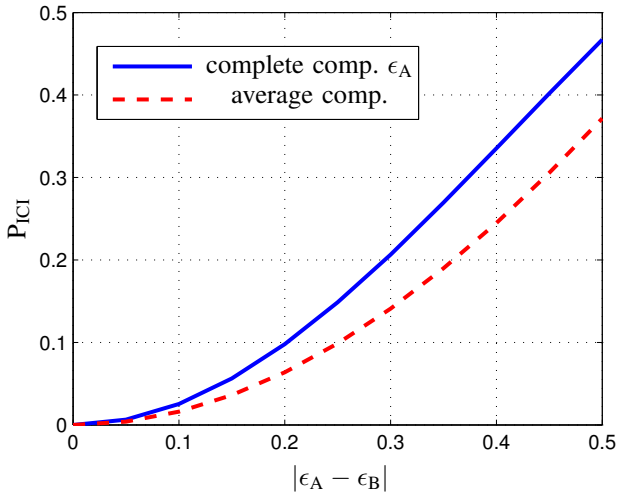

Fig. 6. Total ICI power P_{ICI} versus relative CFO $|\epsilon_A - \epsilon_B|$ after both complete CFO compensation of ϵ_A and average CFO compensation, respectively.

B. ICI Cancelation

Subsequently, ICI cancelation (ICIC) is performed in frequency domain after initial detection for the APP-based decoding schemes. In general, the ICI components presented in (2b) are reconstructed using the estimated individual messages and subtracted from the receive signal. Then the decoding is performed again with respect to the ICI reduced signal. Note that since JCNC only produces the relay codeword $\mathbf{c}_R$ without

ISBN 978-3-8007-3584-6

explicit estimation of $\hat{\mathbf{c}}_\mathrm{A}$ and $\hat{\mathbf{c}}_\mathrm{B}$, ICIC is not applicable for this scheme. For P-SCD and G-JCNC, the individual source messages are firstly estimated before $\mathbf{c}_\mathrm{R}$ at the relay, which can be used to perform ICIC given by

$$\tilde{\mathbf{y}}_\mathrm{R} = \mathbf{y}_\mathrm{R} - \overline{\mathbf{\Lambda}}_\mathrm{A}\hat{\mathbf{x}}_\mathrm{A} - \overline{\mathbf{\Lambda}}_\mathrm{B}\hat{\mathbf{x}}_\mathrm{B} \tag{5a}$$

$$= \mathbf{\Lambda}_\mathrm{A}\mathbf{x}_\mathrm{A} + \mathbf{\Lambda}_\mathrm{B}\mathbf{x}_\mathrm{B} + \mathbf{n}_\mathrm{R} + \overline{\mathbf{\Lambda}}_\mathrm{A}(\mathbf{x}_\mathrm{A} - \hat{\mathbf{x}}_\mathrm{A}) + \overline{\mathbf{\Lambda}}_\mathrm{B}(\mathbf{x}_\mathrm{B} - \hat{\mathbf{x}}_\mathrm{B}) \; . \tag{5b}$$

Here, $\hat{\mathbf{x}}_i$ denotes the estimate of the source symbol vector at the relay. For ease of notation, (2) denotes here the system equation after CFO compensation. Inserting (2b) into (5a), it can be observed that the ICI reduced signal contains the ICI free signal without CFO mismatch and the remaining ICI, as shown in the first line and second line of (5b), respetively. Note that this ICIC process can be performed iteratively to further improve the performance, as shown in Fig. 7 for the block diagram of P-SCD and G-JCNC with CFO compensation and ICIC. As the iteration number increases, less amount of remaining ICI leads to reduced impairment.

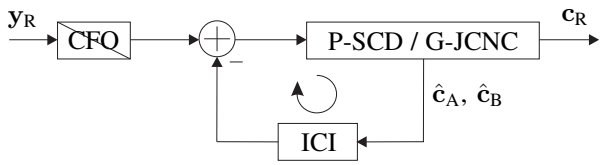

Fig. 7. Block diagram of P-SCD and G-JCNC with CFO compensation and ICIC at the relay. The ICIC process can be performed iteratively.

For S-SCD with CFO compensation and ICIC, a modified S-SCD scheme is developed with the block diagram shown in Fig. 8. After an initial CFO compensation, the codeword from the stronger link, e.g., $\hat{\mathbf{c}}_\mathrm{A}$, is estimated. Subsequently, the ICI as well as the desired signal regarding $\hat{\mathbf{x}}_\mathrm{A}$ is subtracted from the receive signal as

$$\tilde{\mathbf{y}}_\mathrm{R} = \mathbf{y}_\mathrm{R} - (\mathbf{\Lambda}_\mathrm{A} + \overline{\mathbf{\Lambda}}_\mathrm{A})\hat{\mathbf{x}}_\mathrm{A} \tag{6a}$$

$$= (\mathbf{\Lambda}_\mathrm{B} + \overline{\mathbf{\Lambda}}_\mathrm{B})\mathbf{x}_\mathrm{B} + \mathbf{n}_\mathrm{R} + (\mathbf{\Lambda}_\mathrm{A} + \overline{\mathbf{\Lambda}}_\mathrm{A})(\mathbf{x}_\mathrm{A} - \hat{\mathbf{x}}_\mathrm{A}) \; . \tag{6b}$$

Assuming correct decoding of the message from source A, i.e., $\hat{\mathbf{x}}_\mathrm{A} = \mathbf{x}_\mathrm{A}$, both the signal and ICI components stemming from $\mathbf{x}_\mathrm{A}$ are completely removed, indicating that the second line of (6b) is equal to $\mathbf{0}$. Since the resulting interference reduced signal contains only the signal contribution from $\mathbf{x}_\mathrm{B}$, the corresponding CFO leading to the ICI term $\overline{\mathbf{\Lambda}}_\mathrm{B}$ can be completely compensated. Thereafter, $\hat{\mathbf{c}}_\mathrm{B}$ is estimated from the ICI free signal by a common decoding. Such an ICIC process together with successive decoding can also be performed iteratively for further performance improvement.

Note that when jointly considering SCD and ICIC, employing S-SCD is more reasonable compared to P-SCD. This is because the signal cancelation for both ICI and successive decoding makes use of the estimated individual message. Therefore, both ICI and the desired signal $(\mathbf{\Lambda}_\mathrm{A} + \overline{\mathbf{\Lambda}}_\mathrm{A})\hat{\mathbf{x}}_\mathrm{A}$ in (6a) can be subtracted from the receive signal simultaneously

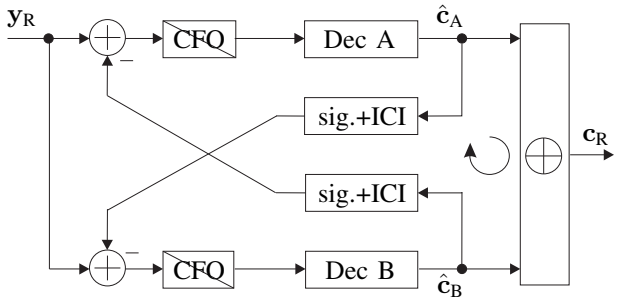

Fig. 8. Block diagram of modified S-SCD with CFO compensation and ICIC at the relay. The ICIC process together with successive decoding can be performed iteratively.

in the modified S-SCD scheme. Whereas in (5a) for P-SCD, only the ICI term $\overline{\mathbf{\Lambda}}_\mathrm{A}\hat{\mathbf{x}}_\mathrm{A}$ is subtracted, leaving $\mathbf{\Lambda}_\mathrm{A}\hat{\mathbf{x}}_\mathrm{A}$ still as 'interference' for re-decoding. On the other hand, P-SCD with iterative ICIC is similar to iterative parallel interference cancelation for multi-user detection, and thus its performance is still evaluated in the next section.

C. Hard vs. Soft Interference Cancelation

As shown in Fig. 7 and Fig. 8, the interference is reconstructed using the hard decided code bits $\hat{\mathbf{c}}_i$ at the relay with $\hat{\mathbf{x}}_i = \mathcal{M}(\hat{\mathbf{c}}_i)$ and subtracted from the receive signal. However, when decoding errors occur, the interference will be estimated erroneously, which leads to error propagation that jeopardizes the decoding performance after such a hard interference cancelation (hIC).

In order to mitigate the performance degradation caused by hIC, reliability information is utilized to estimate $\hat{\mathbf{x}}_i$ for the calculation in (5) and (6), which is termed soft interference cancelation (sIC) [12]. For the sake of illustration, BPSK modulation is assumed with the mapping rule $\hat{\mathbf{x}}_i = \mathbf{1} - 2 \cdot \hat{\mathbf{c}}_i$. Note that extension to higher modulation schemes are straightforward. Correspondingly, the estimated source symbol $\hat{x}_{i,m}$ on subcarrier m (subscript m will be omitted in the sequel for ease of notation) is given by the soft bit as

$$\hat{x}_i = \tanh\left(\frac{L_i}{2}\right) \; , \tag{7}$$

where L_i represents the log-likelihood ratio (LLR) after soft-input soft-output channel decoding for SCD. When G-JCNC is applied, the APPs are directly updated in a non-binary channel decoder. Denoting $P_{c_\mathrm{A}c_\mathrm{B}}$ the APP $\Pr\{(c_\mathrm{A}, c_\mathrm{B})|y_\mathrm{R}\}$ that the bit tuple $(c_\mathrm{A}, c_\mathrm{B})$ is transmitted conditioned on receiving y_R, the estimated source symbols are determined by

$$\hat{x}_\mathrm{A} = (P_{00} + P_{01}) \cdot 1 + (P_{10} + P_{11}) \cdot (-1) \tag{8a}$$

$$\hat{x}_\mathrm{B} = (P_{00} + P_{10}) \cdot 1 + (P_{01} + P_{11}) \cdot (-1) \; . \tag{8b}$$

The soft source symbol $\hat{x}_i \in (-1, 1)$ in (7) and (8) approaches ± 1 when the corresponding code bit c_i is correctly decoded with high probability, which is equivalent to hIC. Otherwise, it approaches 0, which implies nearly no interference cancelation regarding this subcarrier wise signal. Thus, the impact of error propagation is mitigated by applying sIC.

ISBN 978-3-8007-3584-6

V. Performance Evaluation

A symmetric two-way relaying network is considered with the three nodes on a line. OFDM with $N_C = 1024$ subcarriers and QPSK modulation is applied to combat multi-path Rayleigh fading with $N_H = 5$ channel taps. The SNR is defined as SNR $= 1/\sigma_n^2$. Each OFDM symbol is encoded by an LDPC code with rate $R_C = 0.5$. A maximum number of 100 iterations is employed for both binary and non-binary LDPC decoding using the sum-product algorithm. Average CFO compensation is applied due to less amount of ICI compared to complete compensation of one CFO, as shown in Fig. 6. Furthermore, sIC is employed for interference cancelation for its robust performance in contrast to hIC.

The bit error rate (BER) of the XORed packet $\mathbf{c}_R$ at the relay for P-SCD is shown in Fig. 9 with relative CFO $|\epsilon_A - \epsilon_B| = 0.4$. Therefore, the corresponding CFO after average compensation yields $\epsilon_i' = \pm 0.2$. As can be observed in the figure, the CFO mismatch results in catastrophic performance without ICIC. However, ICIC improves the performance significantly with increasing number of iterations. Specifically, the improvement converges at the third iteration, which amounts to only 2 dB loss compared to the case without CFO at BER $= 10^{-3}$.

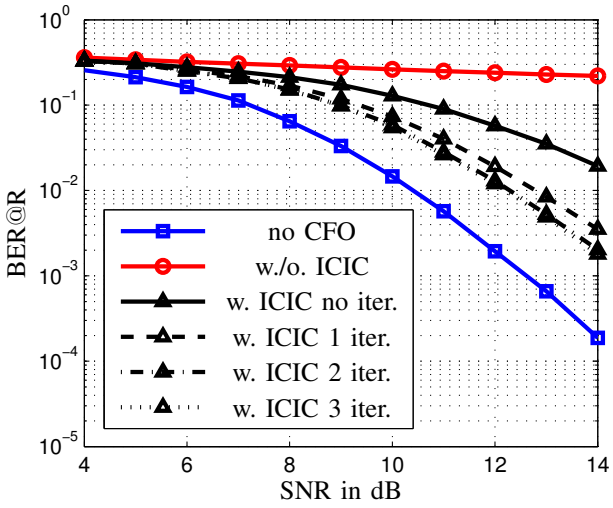

Fig. 9. BER of the XORed packet at relay R for P-SCD with relative CFO $|\epsilon_A - \epsilon_B| = 0.4$ and average CFO compensation, leading to $\epsilon_i' = \pm 0.2$. sIC without and with 1,2 and 3 iterations is employed for ICIC.

The scenario shown in Fig. 9 is reconsidered for the relative CFO equal to $|\epsilon_A - \epsilon_B| = 0.2$ in Fig. 10. In this case, the CFO mismatch still leads to more than 2 dB loss compared to the case without CFO even at BER $= 10^{-2}$. It can be also observed that the presented ICIC strategy works effectively, which approaches the case without CFO with only a very slight performance degradation. Additionally, the performance improvement provided by further iterations for ICIC is almost negligible, indicating that ICIC with no iteration seems to be sufficient in this case when $|\epsilon_A - \epsilon_B| = 0.2$.

The BER performance for the modified S-SCD scheme is shown in Fig. 11 with $|\epsilon_A - \epsilon_B| = 0.2$. Note that the iterations

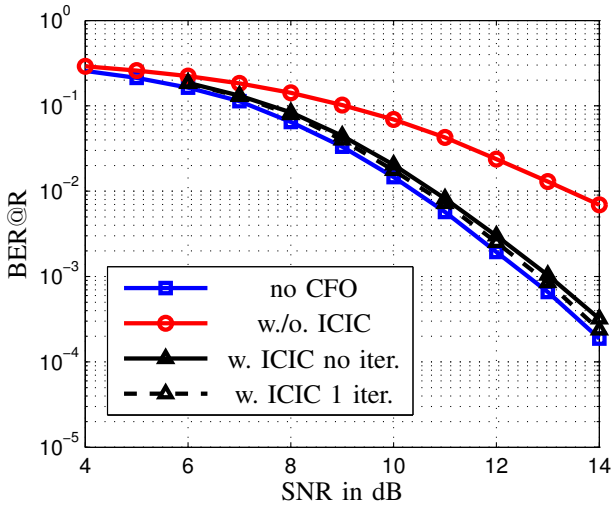

Fig. 10. BER of the XORed packet at relay R for P-SCD with relative CFO $|\epsilon_A - \epsilon_B| = 0.2$ and average CFO compensation, leading to $\epsilon_i' = \pm 0.1$. sIC without and with 1 iteration is employed for ICIC.

herein are regarding to both ICIC and successive decoding for S-SCD. As presented in [3] and verified here by comparing to Fig. 10, basically, S-SCD leads to superior performance in contrast to P-SCD. Still a significant performance loss is observed when ICIC is not applied. Similar to the previously shown results, ICIC for modified S-SCD also improves the BER dramatically, which approaches the case without CFO within 1 dB loss after the first iteration.

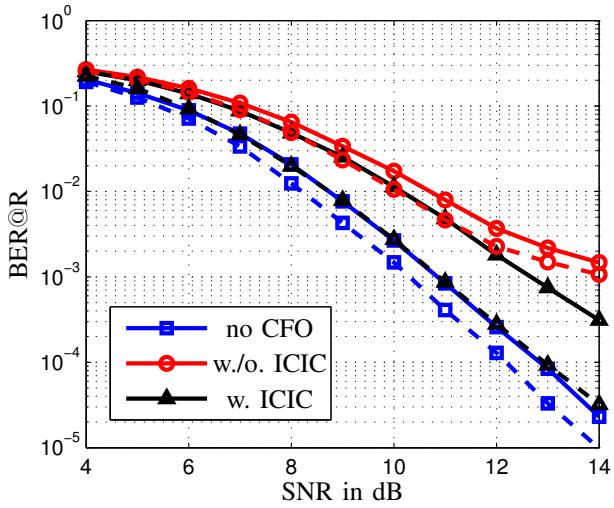

Fig. 11. BER of the XORed packet at relay R for modified S-SCD with relative CFO $|\epsilon_A - \epsilon_B| = 0.2$ and average CFO compensation before initial detection, leading to $\epsilon_i' = \pm 0.1$. sIC without iteration (solid lines) and with 1 iteration (dashed lines) is employed for both ICIC and successive decoding.

For G-JCNC, the corresponding BER performance is shown in Fig. 12 with $|\epsilon_A - \epsilon_B| = 0.2$. As observed in the figure, G-JCNC is the most robust scheme against CFO mismatch compared to P-SCD in Fig. 10 and modified S-SCD in Fig. 11

ISBN 978-3-8007-3584-6

without ICIC, which shows only a 1 dB loss to the case without CFO at BER $= 10^{-3}$. Furthermore, ICIC with no iteration already leads to significantly improved performance by approaching the case without CFO with a slight dB loss.

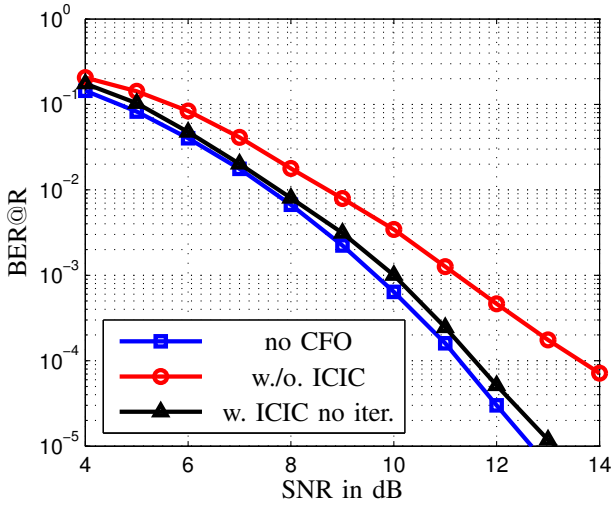

Fig. 12. BER of the XORed packet at relay R for G-JCNC with relative CFO $|\epsilon_A - \epsilon_B| = 0.2$ and average CFO compensation, leading to $\epsilon_i' = \pm 0.1$. sCIC without iteration is employed for ICIC.

VI. Hardware Implementation

For the real-time transmission with PLNC, a radio-frame has to be defined, which should contain synchronization signals and pilots for the channel estimation. Furthermore, the OFDM parameters have to be matched to the available hardware resources in the transmission environment. In this section, hardware implementation for the MA phase of two-way relaying networks with PLNC is demonstrated, where the frame structure is introduced first. Subsequently, the OFDM parameters are discussed and finally the hardware demonstrator is briefly explained.

A. Radio-Frame Structure

The radio-frame definition is inspired by the LTE standard [13]. Due to the embedded sampling clocks in the hardware

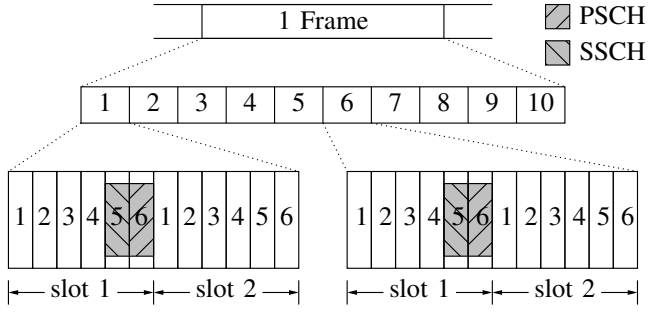

Fig. 13. Schematical illustration of the frame structure with embedded synchronization signals.

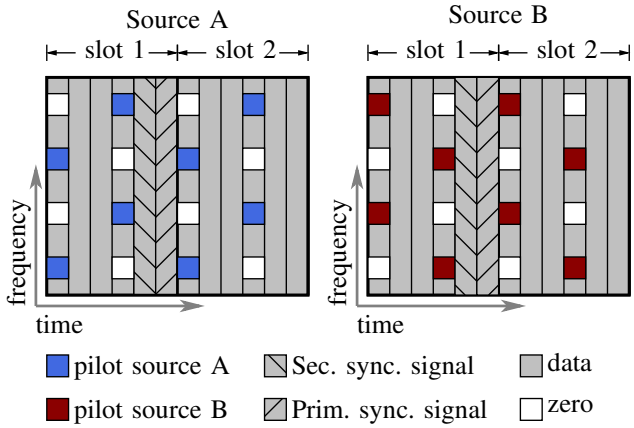

Fig. 14. Time-frequency grid of the frames of sources A and B for the two-phase scenario with orthogonal pilot pattern.

demonstrator some modifications are accomplished to avoid the use of an additional external clock. The defined radio frame has a duration of $T_{\text{frame}} = 30.7$ ms containing 10 subframes. Therefore, each subframe is split into two slots as is shown in Fig. 13, whereas each slot contains 6 OFDM symbol vectors so that the whole frame consists of 120 OFDM symbol vectors. For synchronization, two different synchronization sequences are embedded in the first slot of the subframes one and six. The primary synchronization signal (PSCH) located in the sixth OFDM symbol vector consists of a Zadoff-Chu-Sequence whereas the secondary synchronization signal (SSCH), which consists of two interleaved M-sequences, is located in the fifth OFDM symbol vector. Both signals are arranged symmetrically around the DC-carrier on 62 subcarriers whereas the remaining subcarriers are set to zero.

Furthermore, for both sources A and B cell specific reference signals are added, which are composed of QPK modulated symbols. This scattered pilots are used for channel estimation and are arranged in an orthogonal pilot pattern because in the MA phase both signals are superimposed. A section of the time-frequency grid of the frames for sources A and B is illustrated in Fig. 14. With this mapping of reference signals the effort of channel estimation can be reduced because the pilots will not be superimposed by interference of signals of the other source.

B. OFDM-Parameters

As mentioned before, the frame structure is inspired by the LTE standard. Furthermore, the OFDM-Parameters are also similar to the LTE standard. The LTE standard defines several transmission modes with different bandwidths (specifically 1.4 MHz, 3 MHz, 5 MHz, 10 MHz, 15 MHz and 20 MHz) and two different lengths of the cyclic prefix (CP). The variation of the bandwidth can be achieved by variation of the numbers of used subcarriers or by the FFT size which is up to 2048. All modes have in common, that they use a subcarrier spacing of 15 kHz. Tab. I shows the fundamental parameters used in this

ISBN 978-3-8007-3584-6

work by the hardware (HW) demonstrator compared to the 1.4 MHz and 20 MHz bandwidth mode of the LTE standard. It has been presented previously, that the embedded oscillator of the HW demonstrator is used for sampling the IQ-data with the analog to digital converters (ADC) and digital to analog converters (DAC). This induces some deviations of the OFDM-parameters compared to the LTE standard. Thereby, the frame duration is increased and the subcarrier spacing is decreased to about 4.88 kHz. Furthermore, LTE defines 43 different frequency bands for transmission [14]. However the front-ends of the HW demonstrator are limited to the 2.4 GHz to 2.5 GHz and 5.2 GHz to 5.8 GHz ISM bands, so that a carrier frequency of $f_c = 2.484$ GHz is chosen.

TABLE I
OFDM AND TRANSMISSION PARAMETERS OF THE 1.4 MHZ AND 20 MHZ BANDWIDTH LTE MODE COMPARED TO PARAMETERS OF THE HW DEMONSTRATOR IN THIS WORK.

Parameter	LTE	HW Demonstrator
Bandwidth	1.4 MHz / 20 MHz	$\approx$ 0.35 MHz
FFT size N_{FFT}	128 / 2048	2048
CP length	32 / 512	512
Frame duration	10 ms	30.7 ms
Used subcarriers N_C	72 / 1200	72
Carrier frequency f_c	-	2.484 GHz
Sampling frequency f_s	1.92 MHz / 30,72 MHz	10 MHz
Subcarrier spacing Δf_{sc}	15 kHz	4.88 kHz
Modulation	QPSK, 16-/64-QAM	QPSK
Channel Code	Turbo code	LDPC code, $R_C = 0.5$

C. Hardware Demonstrator

For real-time transmission, the two-way relaying network is implemented in a hardware demonstrator environment. The sources A, B and the relay R are implemented on identical Lyrtech communications systems [11]. This platform is a flexible hardware system, which can be used for many MIMO transmission scenarios. The front-ends consist basically of the radio frequency (RF) transceiver chips MAX2829 [15] and analog to digital as well as digital to analog converters (ADC/DAC). The baseband processing can be done partitioned to several field-programmable gate arrays (FPGAs) and powerful digital signal processors (DSPs).

A block diagram of the receive path at relay R is illustrated in Fig. 15. At first, the continuous receive signal at the antenna is amplified to match the signal power to the receiver input limits. The down-conversion of the signal into the baseband domain is done by a mixer, which is controlled by the local oscillator. Since this oscillator has a finite accuracy and also the mixer is non ideal, the complex baseband signal will not be exactly centered at 0 Hz. This mismatch is the CFO on the receiver side at the relay. Furthermore, the front-ends in both sources A and B induce a CFO. After generating the

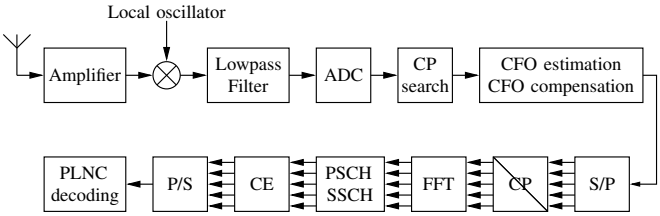

Fig. 15. System block diagram for hardware implementation of the receiver at relay R.

baseband signal, it is filtered by a lowpass filter and is sampled by an ADC with the sampling frequency $f_s = 10$ MHz. Subsequently, the CPs of the superimposed OFDM signals of sources A and B will be detected by a cross-correlation. With the detected CP positions the average CFO is estimated in the time-domain by calculating the phase difference between the CP and the corresponding parts of the OFDM symbol vector. In the following, the estimated average CFO is compensated and the serial data is converted into parallel OFDM symbol vectors. After removing the CPs and applying FFT to the resulting signal, the synchronization signals PSCH and SSCH will be detected by another cross-correlation to determine the beginning and end of the received frame. The channel effects are compensated by the channel equalizer (CE), which uses a pilot based linear channel estimation. Furthermore, the pilots are removed and the remaining QPSK symbols are converted to a serial sequence. Finally, the PLNC decoding is performed using the APP-based schemes presented in Section III. If the ICIC is applied this is embedded in the PLNC decoding block.

D. Measurement Results

In this section, measurement results are presented, for which the described HW demonstrator is used in a symmetric two-way relaying network. For all measurements the noise power is insignificant compared to the signal power because not the performance compared to the SNR is observed but rather the performance compared to the CFO. However, this work only focuses on the CFO, such that all other impairments of the front-ends were not analyzed and compensated. The most important impairments are sampling clock offset, sampling clock jitter, IQ-imbalance, non-linear power amplifiers and phase noise [16]. Due to these non-ideal conditions, the performance is decreased compared to the simulation results presented before. Furthermore, only a simple least square channel estimation with a linear interpolation is performed.

Fig. 16 shows the superimposed QPSK constellation received at relay R after removing the average CFO without ICIC. The average CFO is determined by the CPs of the superimposed OFDM symbol vectors. For lower relative CFOs the constellation points can be clearly separated, whereas for higher relative CFOs this is getting more difficult.

The measured BER of the XORed packet $\mathbf{c}_R$ at the relay for JCNC, S-SCD and G-JCNC is shown in Fig. 17. Note that P-SCD is omitted because of its inferior performance in contrast to S-SCD. Instead of that the BER of JCNC, which can not

ISBN 978-3-8007-3584-6

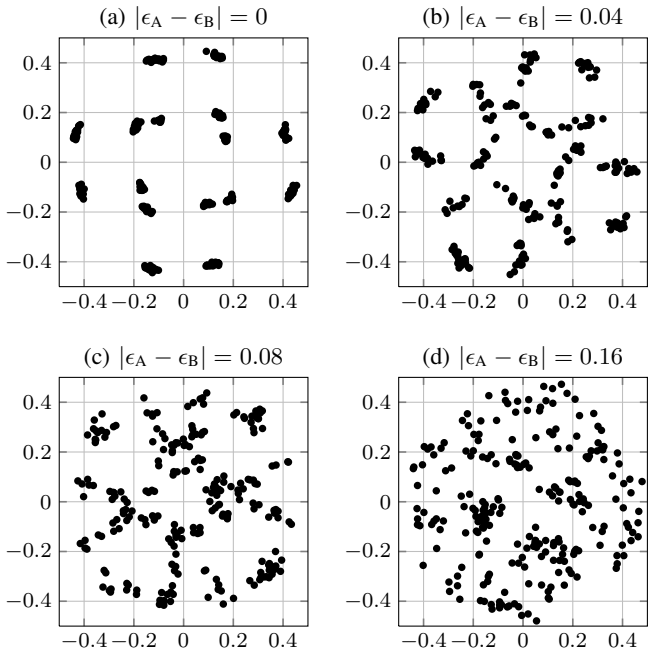

Fig. 16. Measured constellation diagram of the superimposed QPSK constellation received at relay R for different relative CFOs and average CFO compensation without ICIC.

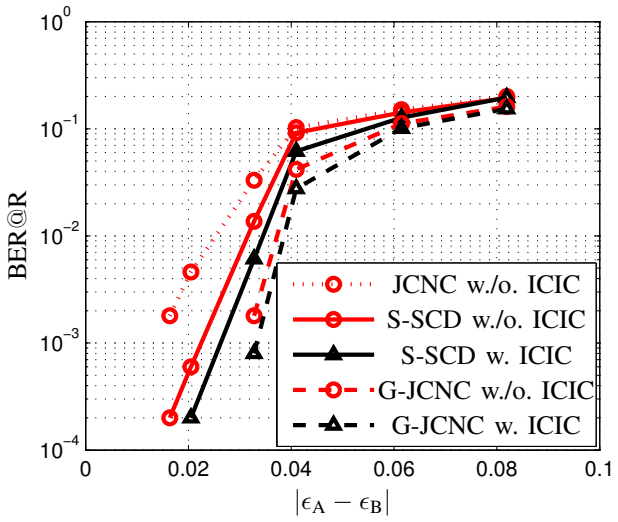

Fig. 17. BER of the XORed packet at relay R from the measurement for JCNC, S-SCD and G-JCNC.

be executed with ICIC, is included for further comparison. For interference cancelation in S-SCD and G-JCNC, ICIC without iteration and sIC are performed. As described before, the measurements should not concentrate on the SNR but are functions of the relative CFO. Similar to the previously shown simulation results in Section V, ICIC improves the BER for all PLNC decoding schemes. As observed in Fig. 17, S-SCD outperforms JCNC and G-JCNC is the most robust scheme against CFO mismatch compared to JCNC and S-SCD irrespective of the application of ICIC.

VII. Concluding Remarks

We studied PLNC with CFO mismatch in the MA phase for two-way relaying networks. Practical CFO compensation and ICI cancelation strategies are presented that mitigate the impairment from CFO mismatch effectively for APP-based PLNC decoders. For hardware implementation, the radio frame structure adapted to PLNC transmission is explained, as well as the basic implementation of the receiver at the relay in the hardware demonstrator. Finally the measurement results of the real-time transmission confirm the presented investigation of the CFO compensation and ICI cancelation strategies. In the future, the influence of further impairments from the front-ends has to be analyzed in the PLNC transmission.

VIII. Acknowledgement

This work was supported in part by the German Research Foundation (DFG) under grant Wu 499/8-1 and Pa 438/6-1 within the priority program ”Communication in Interference Limited Networks (COIN)”, SPP 1397.

References

[1] S. Zhang, S. C. Liew, and P. P. Lam, “Hot Topic: Physical-Layer Network Coding,” in *International Conference on Mobile Computing and Networking (MobiCom’06)*, Los Angeles, CA, USA, Mar. 2006.

[2] S. Zhang and S. C. Liew, “Channel Coding and Decoding in a Relay System Operated with Physical-Layer Network Coding,” *IEEE Journal on Selected Areas in Communications*, vol. 27, no. 5, pp. 788–796, Oct. 2009.

[3] D. Wübben and Y. Lang, “Generalized Sum-Product Algorithm for Joint Channel Decoding and Physical-Layer Network Coding in Two-Way Relay Systems,” in *IEEE Global Communications Conference (GLOBECOM’10)*, Miami, FL, USA, Dec. 2010.

[4] V. Kotzsch, J. Holfeld, and G. Fettweis, “Joint Detection and CFO Compensation in Asynchronous Multi-User MIMO OFDM Systems,” in *IEEE 69th Vehicular Technology Conference (VTC-Spring’09)*, Barcelona, Spain, Apr. 2009.

[5] M. Schellmann and V. Jungnickel, “Multiple CFOs in OFDM-SDMA Uplink: Interference Analysis and Compensation,” *EURASIP Journal on Wireless Communications and Networking*, vol. 2009, Apr. 2009.

[6] D. Marabissi, R. Fantacci, and S. Papini, “Robust Multiuser Interference Cancellation for OFDM Systems with Frequency Offset,” *IEEE Transactions on Wireless Communications*, vol. 5, no. 11, Nov. 2006.

[7] J. A. Fessler and A. O. Hero, “Space-Alternating Generalized Expectation-Maximization Algorithm,” *IEEE Transactions on Signal Processing*, vol. 42, no. 10, Oct. 1994.

[8] J. H. Lee and S. C. Kim, “Time and Frequency Synchronization for OFDMA Uplink System using the SAGE Algorithm,” *IEEE Transactions on Wireless Communications*, vol. 6, no. 4, Apr. 2007.

[9] Ettus Inc., “Universal Soft Radio Peripheral,” http://www.ettus.com/.

[10] L. Lu, T. Wang, S. C. Liew, and S. Zhang, “Implementation of Physical-Layer Network Coding,” in *IEEE International Conference on Communications (ICC’12)*, Ottawa, Canada, Jun. 2012.

[11] Nutaq Inc., “LYRtech,” http://www.nutaq.com/.

[12] X. Wang and V. Jungnickel, “Iterative (Turbo) Soft Interference Cancellation and Decoding for Coded CDMA,” *IEEE Transactions on Communications*, vol. 47, no. 7, Jul. 1999.

[13] 3GPP, “Technical Specification Group Radio Access Network; Evolved Universal Terrestrial Radio Access (E-UTRA); Physical channels and modulation (Release 12),” [Online]. Available: http://www.3gpp.org/ftp/Specs/html-info/36211.htm, Dec. 2013.

[14] S. Sesia, I. Toufik, and M. Baker, *LTE - The UMTS Long Term Evolution: From Theory to Practice*, Wiley, 2011.

[15] Maxim Integrated, “MAX2828, MAX2829 - Single-/Dual-Band 802.11a/b/g World-Band Transceiver ICs,” http://datasheets.maximintegrated.com/en/ds/MAX2828-MAX2829.pdf.

[16] F. Horlin and A. Bourdoux, *Digital compensation for analog front-ends: a new approach to wireless transceiver design*, J. Wiley & Sons, 2008.

ISBN 978-3-8007-3584-6